Exploring the potential location of future earthquakes in Harrat Lunayyir, Western Saudi Arabia

Ali Abdelfattah, Chokri Jallouli, Hassan Alzahrani, Saleh Qaysi, Mohammed Fnais & Abdullah Al-Amri

Published online: 20 Jan 2025.

Submit your article to this journal ↗

Article views: 4

View related articles ↗

View Crossmark data ↗

Taylor & Francis
Taylor & Francis Group

RESEARCH ARTICLE

∂ OPEN ACCESS   Check for updates

Exploring the potential location of future earthquakes in Harrat Lunayyir, Western Saudi Arabia

Ali Abdelfattah ⃝iD, Chokri Jallouli, Hassan Alzahrani, Saleh Qaysi, Mohammed Fnais and Abdullah Al-Amri

Department of Geology & Geophysics, King Saud University, Riyadh, Kingdom of Saudi Arabia

ABSTRACT

The Arabian Shield constitutes the eastern flank of the Red Sea and features zones rich in lava flows potentially associated with seismic activity. Notably, the Harrat Lunayyir (HL) seismic dislocation zone in the shield experienced a prominent earthquake swarm in 2009, representing seismic activity that may have induced subsequent Coulomb stress changes and gravity anomalies. Integrating analyses of gravity anomalies, earthquake characteristics, and Coulomb stress transfers were performed to explore the variations in static stress and depth-dependent crustal heterogeneities. The spatial distribution of hypocentres, seismic moment, focal mechanisms, and frictional properties demarcates the weakness subzone in HL bordered by hardness zones. Coulomb stress analysis identified positive stress patterns aligned with a north-northwest (NNW) trend, parallel to the Red Sea rift axis, while negative stress patterns were distributed both eastward and westward. Gravity modelling highlighted crustal heterogeneities with low-density areas corresponding to the seismic activity zone and high-density regions in the surrounding vicinity. A significant correlation between observed anomalies and the NNW faults elucidates the regional tectonic processes within the Red Sea rifting system. The highlighted fault segments and depth-dependent crustal heterogeneities may pose considerable seismic hazard potentials in the region, emphasising the necessity for ongoing monitoring and assessment.

1. Introduction

A significant challenge in the field of seismology concerns predicting future seismic events. Recent studies have indicated that changes in static stress are instrumental in influencing the occurrence of future earthquakes. Conversely, the mode of earthquake rupture is significantly affected by numerous small-scale ruptures, including barriers and asperities, which arise from the crustal heterogeneities in the earthquake dislocation zones. This study provides cartographic representations illustrating the alterations in static stress and the crustal heterogeneities within and surrounding the Harrat Luynnier (HL) seismic dislocation zone. Analysing the interactions among crustal heterogeneities, seismic activity, and Coulomb stress is essential for identifying regions vulnerable to future earthquakes, thereby facilitating the development of risk mitigation strategies. Various geophysical methods, including gravity analysis, seismic tomography, and receiver function analysis, are employed to elucidate crustal heterogeneities. Investigating variations in crustal density and the spatial distribution of earthquakes on a localised scale is vital for comprehending crustal heterogeneity, as evidenced by prior studies

(Abdelfattah et al., 2017; Bhattacharya & Kayal, 2003; Khan & Chakraborty, 2007). In Alkan et al. (2023), shear velocity, b-value, and Coulomb stress changes were calculated and correlated with local seismicity. Furthermore, in addition to the analysis of Coulomb failure stress, geophysical techniques such as gravity modelling are applied to assess crustal thickness and velocity structure, which are pivotal for a comprehensive understanding of earthquake rupture dynamics.

Coulomb failure stress is fundamental to comprehend earthquake mechanics, as it pertains to the shear stress necessary for fault slip and subsequent earthquake occurrence. It plays a crucial role in elucidating seismic phenomena, including earthquake swarms; however, the complexities associated with stress changes and fault dynamics in swarm environments continue to be a subject of debate. The investigation conducted by Harris (1998) highlighted the influence of stress variations from prior seismic events on the likelihood of future earthquakes. Aoyama et al. (2000) employed Coulomb stress analysis to examine the Hida swarm in Japan, thereby demonstrating the method's effectiveness in enhancing the understanding of

swarm development. Changes in static stress not only dictate the timing of earthquakes but also significantly impact rupture characteristics. As documented by Stein et al. (1997), observations from the North Anatolian Fault sequence underscore the critical role that stress interactions play in the dynamics of earthquakes. Although static stress changes have been extensively documented along established fault lines, a comprehensive understanding of these changes within intricate systems like swarms, such as the Hida swarm, necessitates sophisticated modelling techniques.

Subsurface heterogeneities within the lithosphere represent a critical aspect of comprehending the occurrence of future earthquakes and their dynamic ruptures. Ongoing studies and advancements in geophysical and geological methodologies enhance our insight into these complex structures, which may arise from features such as asperities and barriers. These heterogeneities significantly influence the distribution and intensity of seismic activity, as the presence of faults and fractures establishes zones of weakness that govern the initiation and propagation of earthquakes. Examining crustal heterogeneities is vital, as they impact the distribution of stress and strain, subsequently affecting the probability and characteristics of seismic events. The roughness of fault surfaces is particularly important, as it plays a significant role in determining frictional behaviour, assessing seismic hazards, and predicting both the probability and magnitude of earthquakes. The interplay between fault roughness and frictional properties substantially contributes to seismic behaviour and the likelihood of future seismic occurrences. The friction coefficient, for instance, affects stress drop and earthquake magnitude; regions characterised by high-friction earthquake source zones typically experience gradual stress accumulation and greater stress release during seismic events. Hence, recognising the importance of crustal heterogeneities and Coulomb failure stress is essential for understanding the spatiotemporal pattern of future earthquake occurrences, as these factors profoundly influence seismic rupture dynamics. This underscores the necessity for precise analysis in the interpretation of seismic processes.

The Red Sea represents a significant active rift system characterised by distinct seismic activity across Egypt and Saudi Arabia. Figure 1 illustrates the major geological features of the Red Sea and the surrounding uplifted margins of the Arabian and Nubian Shields. The Arabian Plate is bordered by several active plate boundaries, which are moving apart from the African Plate, leading to the expansion of the seafloor in the Red Sea through a process known as seafloor spreading. Seismic events occurring inland, particularly in Saudi Arabia, are associated with the enrichment of basaltic flows due to volcanic

eruptions. The intricate geodynamic interactions in this region, which integrate magmatic and tectonic processes, culminated in a notable earthquake swarm (unrest) in the Harrat Luynnier (HL) region in May 2009. A significant earthquake with a moment magnitude (Mw) of 5.4 occurred, which is substantial enough to be considered atypical for standard swarm activities (Abdel-Fattah et al., 2014). Given the rapid development of infrastructure and population growth in the area, it is imperative to conduct further studies to enhance our understanding of seismic hazards in this region. Notably, major cities along the Red Sea coast have experienced considerable and swift development recently, prompting the need for a more comprehensive assessment of seismic risk in this specific area. One critical parameter that influences seismic hazard evaluation is the potential location of future earthquakes. This study focuses on the HL seismic dislocation zone by examining the change in static stress and subsurface crustal heterogeneities. The change in static stress will be assessed using the Coulomb stress failure methodology, while the crustal heterogeneities will be analysed based on lateral variations in density derived from gravity studies. The current study is instrumental in identifying probable locations for future seismic events, as understanding the mechanisms of crustal variation and stress concentration in seismogenic zones can elucidate the occurrence of earthquake hazards in the region. Ultimately, this study aims to anticipate how crustal heterogeneities and Coulomb failure stress interplay to influence the likelihood of future earthquakes in the HL seismogenic zone.

2. Geological and tectonic settings

The Harrat Luynnier (HL) region is located in the western part of Saudi Arabia, onshore the Red Sea coastline, within the Arabian Shield that is recognised as one of the most significant igneous provinces in continental regions globally (Zaidi & Mukhopadhyay, 2015). This area exhibits a wealth of monogenetic volcanic activity, characterised by extensive alkali basalt lava flows and approximately 50 volcanic cones. Various lava flows radiate in multiple directions across the landscape. These volcanic formations are situated directly atop the deeply eroded Neoproterozoic rocks of the Arabian Shield (Johnson, 2006). Volcanic activity in the HL region commenced during the Late Oligocene and Early Miocene epochs and continued into the Quaternary period. Historical records indicate that the most recent eruptions occurred between the 13th century BCE and approximately 600 CE (Johnson, 1998). The geological map presented in Figure 2 shows a complex and a very heterogene Precambrian basement with geological features oriented along two main directions: northwest-southeast (NW-SE) and
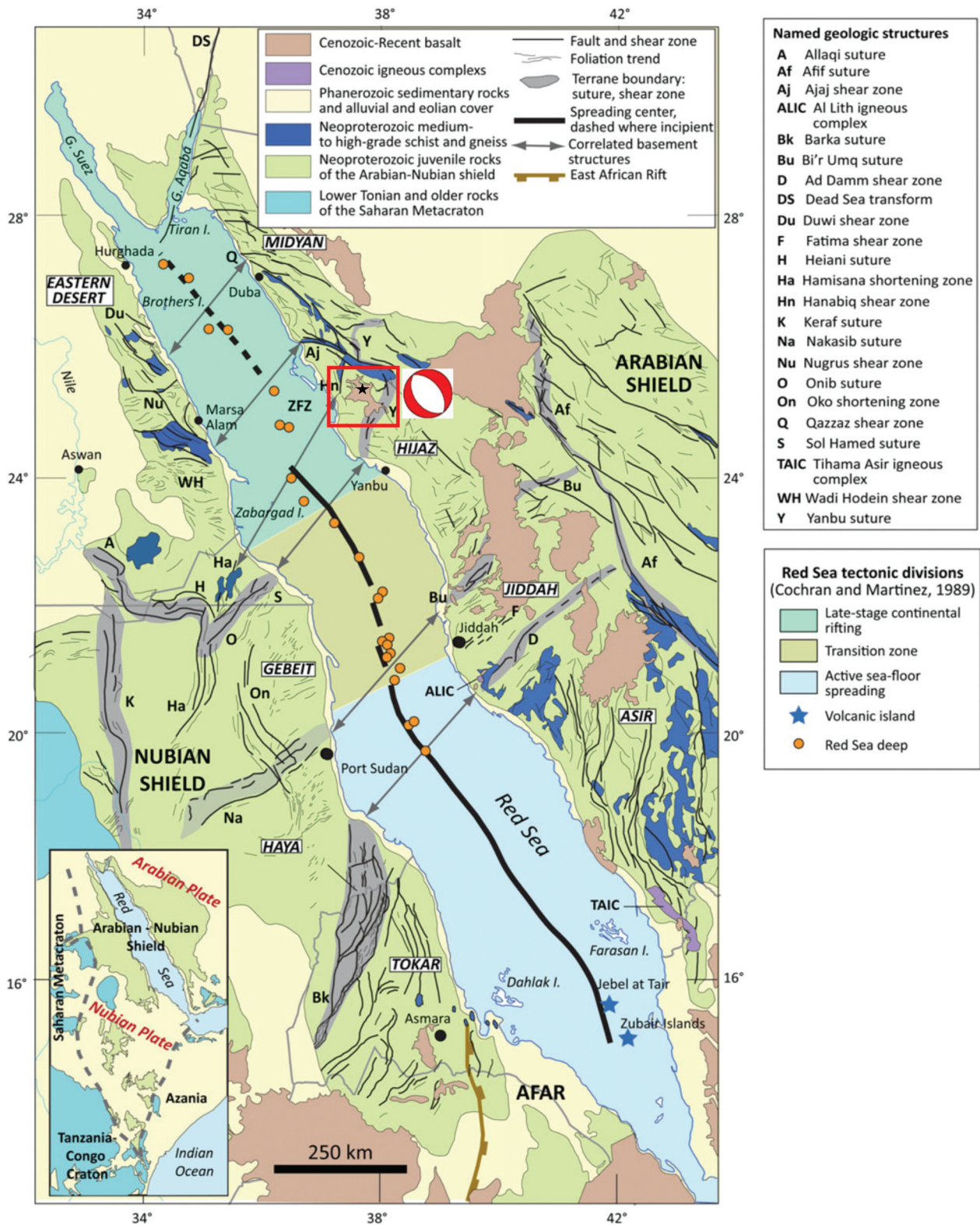
Figure 1. Major geologic features of the Red Sea and surrounding uplifted margins of the Arabian and Nubian shield (Stern & Johnson, 2019). The red square indicates the study area (HL), the black star marks the epicentre of the earthquake of Mw = 5.4 and its source mechanism solution of normal faulting is represented by a red beach ball.

southwest-northeast (SW-NE). The basement is overlain in the centre of the map by the Cenozoic volcanic rocks known by Harrats. The region frequently displays dykes, normal faults, and thin sediment layers aligned with the NW-SE direction, which are associated with the Cenozoic extensional event and the formation of the Red Sea. NW-SE dykes and faults are evidenced by the magnetic anomalies (Abdelfattah et al., 2021). Among the SW-NE geological features those observed inside the blue square (Figure 2) represented by peridotite and serpentinite rocks which constitute a portion of the Precambrian basement.
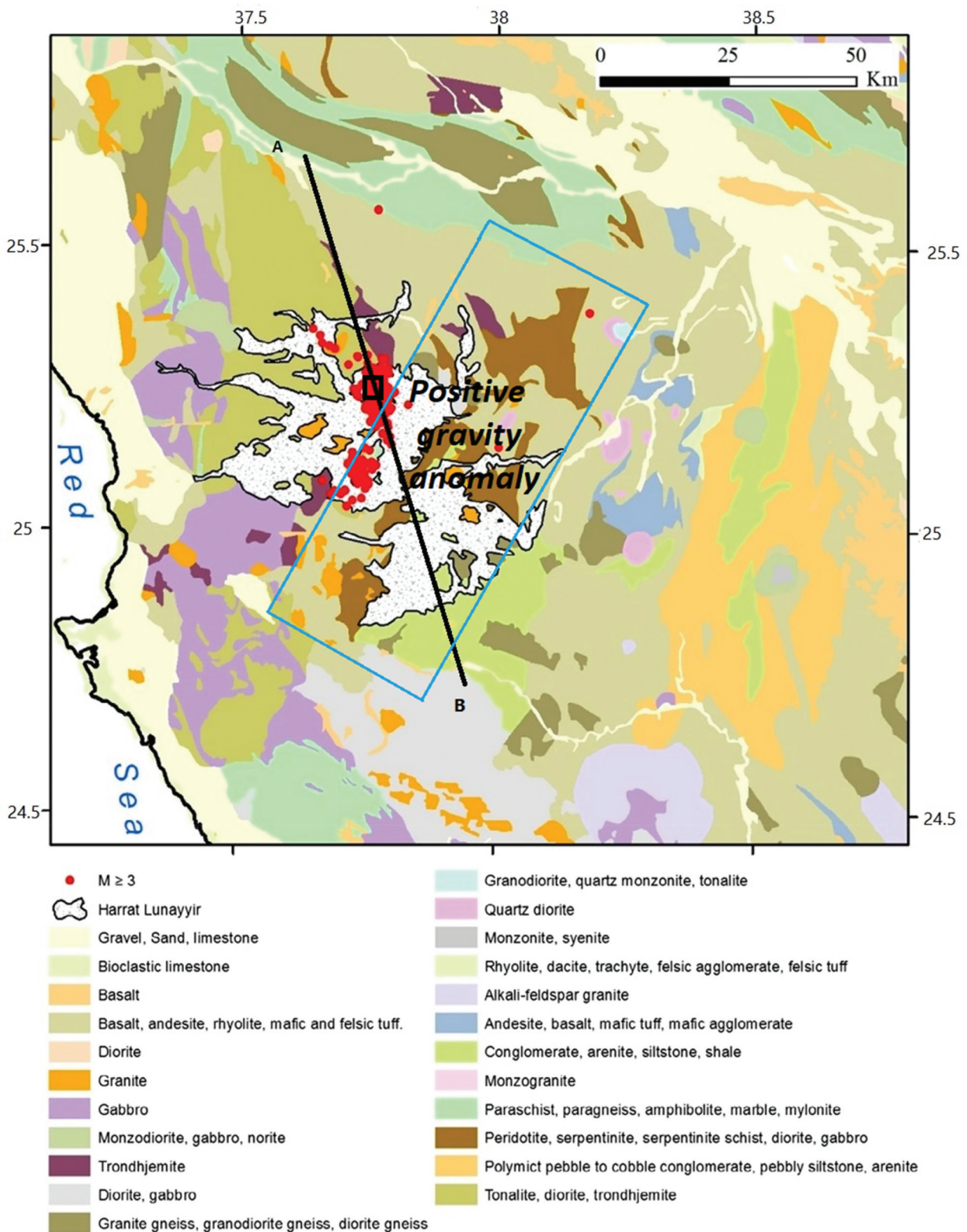
Figure 2. A map showing the geographical distribution of surface geology in the study area (after Saibi et al., 2019). The blue square represents location of the positive gravity anomaly observed in figure 7. The small black square represents location of the picture shown in figure 3. The thick black line (AB) represents location of the modelled gravity profile.

Following comprehensive field surveys conducted shortly after the main shock (Fnais et al., 2010;), the epicentral region displayed a surface rupture trending northwest (NW) associated with the 2009 earthquake series, with a rupture length extending to 8 kilometres. This rupture exhibited local vertical offsets exceeding 1 metre and extended several metres in depth (Figure 3). To model the crustal deformation associated with the seismic activity in the Harrat Luynnier (HL) region, a vertical dike intrusion aligned in a north-northwest to south-southeast (NNW-SSE) orientation was utilised (Baer & Hamiel, 2010; Pallister et al.,

Figure 3. Surface rupture associated with the 2009 earthquake swarm in Harrat Lunayyir (HL). The location of this picture is indicated by the thick black rectangular inset in figure 2.

2010). B. Mukhopadhyay et al. (2012) also noted an initial stage of dike intrusion during this period. During the earthquake swarm of 2009, seismic activity was initially characterised by larger magnitude events occurring at greater depths, subsequently migrating upward to the location of the significant event with a moment magnitude of 5.4 (Abdel-Fattah et al., 2014), followed by smaller tremors occurring to the east. This sequence of unrest provides valuable insights into the dynamics of self-potential rupture and crustal heterogeneities. Recent studies highlight the relationship between the distribution of seismic activities and geological features, including dykes, faults, barriers, and asperities (Harris, 1998; Schoenball & Gröner, 2016). Furthermore, the crustal heterogeneities within the HL region contribute to the roughness of the area where seismic events transpire, which may be attributable to the intrusion of magmatic activity into the upper layers of the Earth's crust (Abdelfattah et al., 2017). A seismic tomography study by Hansen et al. (2013) indicated that dyke intrusions of high velocity extended obliquely upward in the NNW direction. Furthermore, recent seismic tomography models (Koulakov et al., 2015) and attenuation studies (Koulakov et al., 2014; Sychev et al., 2016) have provided insights into the mechanisms of magma and fluid propagation within the region. Zobin et al. (2013) proposed two scenarios suggesting that a volcanic eruption at HL is improbable: one scenario posits that the subsurface intrusion was halted, while the other suggests that the dike was injected along the rift zones.

3. Data use

The waveform recordings utilised in this study were obtained from a nearby seismic network installed by the Saudi Geological Survey (SGS) and King Abdulaziz City of Science and Technology (KACST) shortly after the initiation of the earthquake sequence in April 2009. This network consists of twenty-two three-component temporary stations and two three-component permanent stations. Each station has Trillium broadband velocity sensors featuring a response range of 0.02 to 120 seconds, a digitiser with a sampling rate of 100 samples per second, and a 142 dB dynamic range for the entire recording system.

The strategic distribution and a substantial number of broadband seismic observations deployed in the epicentral area immediately after the onset of the foreshocks of the earthquake unrest in April 2009 provided a valuable opportunity to discern whether the seismic activity in HL resulted from tectonic or magmatic processes. In April 2009, the Saudi Geological Survey (SGS) established several permanent broadband seismic stations in the HL following a surge in seismic activity. Additionally, shortly after the mainshock on May 19, King Abdulaziz City for Science and Technology (KACST) and King Saud University (KSU) deployed temporary seismic networks in HL from May 20 to the end of July 2009 to monitor and analyse aftershock activities. The KACST seismic network comprised 10 short-period, single-component (vertical) seismic stations and one broadband station, while the KSU network included eight short-period seismic stations configured similarly to those of KACST. Each short-period seismic station had an SS-1 seismometer, a Quanterra Q330 digitiser for seismic data logging, a 20GB Baler for data storage, a 12-volt battery, and a solar panel for continuous charging. The broadband stations utilised Streckeisen STS-2 seismometers. Data from broadband and short-period stations are digitised at 300 samples per second (SPS). The temporary seismic network significantly enhanced station coverage over the epicentre area (Al-Zahrani et al., 2012).

The data that represents the parameters of hypocentre and fault plane solutions was collected from Abdelfattah et al. (2017) and Abdelfattah et al. (2020), respectively. The hypocentre relocations, refined by Hansen et al. (2013) and Abdelfattah et al. (2017), revealed a distinct alignment of foreshocks along the western edge of the seismic activity. The hypocentral parameters for approximately 4,986 earthquakes, with magnitudes ranging from −1 to 5.4, were determined between May 13 and 7 June 2009. These relocations delineated a trend along the NNW-SSE direction parallels to the Red Sea. Three distinct phases were identified within the seismic activity, with one cluster displaying shallower focal depths in the mainshock rupture area. The other two clusters were characterised by deeper focal depths compared to the mainshock hypocentre area, representing preshocks and aftershocks, as illustrated in Figure 4. In addition to seismic data, we used gravity data to image the crustal density distribution. We extracted the Bouguer gravity
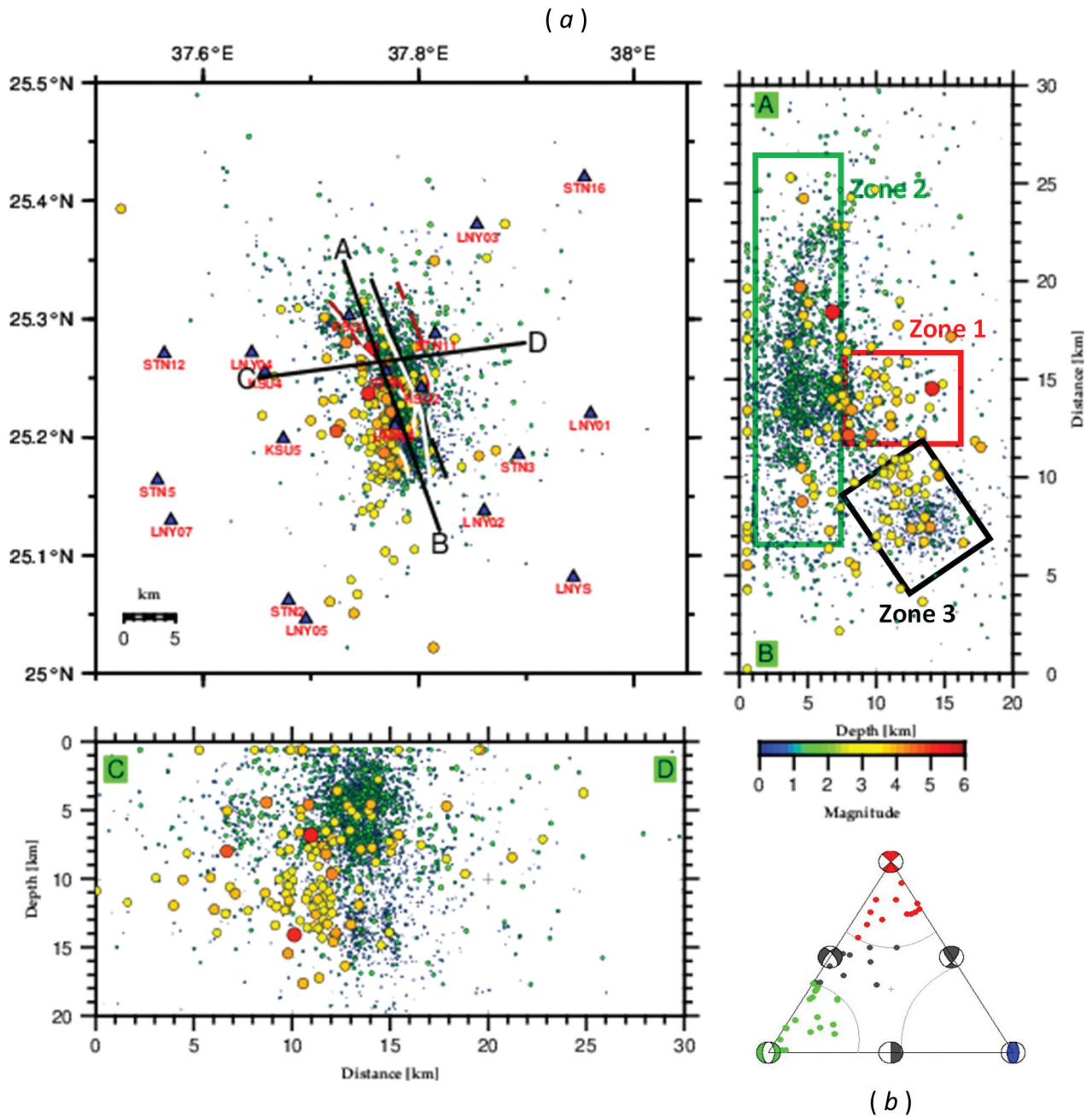
Figure 4. A plot displays (*a*) the spatial distribution map of epicentres as a function of earthquake magnitudes and the cross-section demonstrating the spatial distribution of hypocentres. Additionally, the plot illustrates the distribution of seismic station locations. The plot indicated that the events with the larger magnitudes in the 2009 earthquake unrest were released at deeper focal depths before releasing the largest event at a focal depth of 6 km. Three zones were delineated to recognise three fault segments with the parameters listed in table 1 that were used in calculating the coulomb stress change. The zones were identified based on the criteria of the spatiotemporal distribution of hypocentres, focal mechanism solutions obtained by Abdelfattah et al. (2021), and (*b*) a triangle diagram of the focal mechanism solutions obtained using the method of Frohlich (2001).

anomalies of the study area from the World Gravity Model (WGM2012 model, Bonvalot et al., 2012), which is helpful in revealing anomalies caused by kilometric-width crustal structures.

4. Seismicity analysis

4.1. Seismic moment and stress drops

We estimate the moment magnitude using the regional M_L-M_w relationship (Mereu, 2020):

$$M_w = 0.69 \, M_L + 0.73, \qquad (1)$$

The seismic moment was calculated using the empirical relation established by Hanks and Kanamori (1979):

$$M_o = 10^{[1.5(M_w + 10.7)]} \qquad (2)$$

In our analysis, we calculated the cumulative seismic moment of seismic events among the earthquake unrest and distributed it spatially over an area divided into square grids, with each cell having dimensions of 2×2 km. Subsequently, we conduct two-dimensional mapping, considering the cumulative seismic moment associated with each cell. This mapping approach visually represents the spatial distribution of cumulative seismic energy across the studied area, revealing a significant range of variation. Figure 5 shows the epicentral and hypocentral distributions of the cumulative seismic moment in the HL seismic dislocation zone.

The spatial distribution of stress-drops that may provide valuable insights into the behaviour of faults within the seismogenic zone, particularly in regions with geological heterogeneities. In such areas, factors like volcanic structures can create barriers and asperities that influence stress drop distributions. The two-dimensional distribution examines how stress drops change across different locations within a region. This pattern is typically represented on a map, with different colours or contours indicating varying stress drop magnitudes in different regions. Analysing the two-dimensional distribution of stress drops can provide insights into
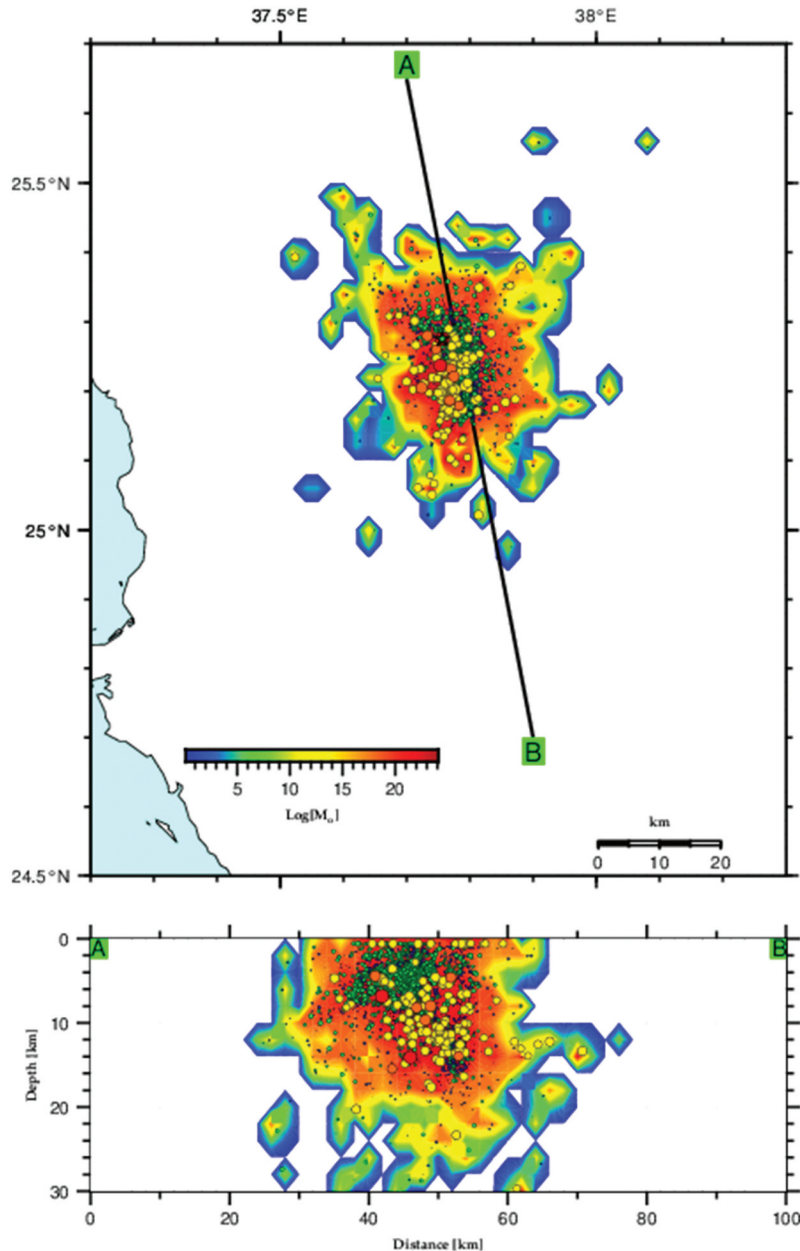

Figure 5. The spatial distribution of seismic moment released during the 2009 earthquake unrest occurred in HL.

the heterogeneities within the seismogenic zone and contribute to a better understanding of seismic activity in a given area. We calculate relative stress drops ($\Delta\tau_{eff}$) among the unrest using methodologies outlined by Chen et al. (2012) and Roland and McGuire (2009) that involve assessing the cumulative seismic moment (ΣMo) released in the activated area (R). According to the stress drop of a single crack (Madariaga & Ruiz, 2016), the effective stress drop can be determined using the following equation;

$$\Delta\tau_{eff} = \frac{7}{16}\frac{\sum^{M_o}}{R^3} \qquad (3)$$

4.2. Coulomb failure stress

Understanding the influence of fault interaction on the regional stress field is crucial for deciphering seismic activity. The 2009 seismic unrest presents an opportunity to investigate the role of fault interaction in producing anomalous focal mechanisms. This analysis aims to verify whether fault interaction significantly alters the background stress field, implying fault interaction on the background stress field and its influence on anomalous focal mechanisms within the 2009 seismic unrest throughout modelling static stress and Coulomb stress changes in the focal zone. The COULOMB 3.3 software developed by Toda et al. (2011) was used to alter the ongoing stress accumulation mechanism, leading to the location of forthcoming earthquakes in the region. This analysis contributes to a better understanding of the complex dynamics of fault systems and their role in seismic events. The calculations are conducted in an elastic half-space with uniform isotropic elastic properties, following the approach outlined by Okada (1992). When an earthquake reduces the average shear stress on the slipped fault, shear stress increases at locations beyond the fault tips. The Coulomb failure stress change, denoted as Δsf, is defined as:

$$\Delta CFF = \Delta\tau + \mu'\Delta\sigma_n$$

This equation quantifies the conditions under which a fault plane will slip and generate an earthquake. Where $\Delta\tau$ is the shear stress change on a fault plane, $\Delta\sigma_n$ is the fault normal stress change, and μ' is the effective coefficient of friction. The friction coefficient values range from 0.0 to 0.8, with 0.4 being commonly employed in calculations (King et al., 1994; Stein et al., 1992), as this value has been commonly used to

minimise uncertainty (Toda & Enescu, 2011; Toda et al., 2011). The value of 0.4 is a commonly employed average friction coefficient that investigates fault slip under varying stress conditions, particularly in relation to the focal mechanisms in the study area, which encompass a combination of normal and strike-slip faulting styles. The geometrical parameters of the specified faults were defined according to Aki and Richards (1980). The rake angle for the focal mechanism solution ranges from −180° to 180°, the strike angle varies from 0° to 360°, and the dip angle ranges from 0° to 90°.

We model the Coulomb stress change associated with the earthquake activity using input parameters for a uniform elastic half-space, including a shear modulus (μ) of 30 GPa and a Poisson ratio of 0.25 (Okada, 1992; Stein et al., 1992; Toda & Stein, 2015). This study employed three fault segments representing three phases in the sequence to compute Coulomb stress failure. Fault parameters such as strike, dip, rake, and friction coefficient, which characterise each segment, were derived from focal mechanism solutions as calculated by Abdelfattah et al. (2021) using stress tensor inversion with the STRESSINVERSE code (Vavryčuk, 2014). The spatial distribution of events representing each rupture stage was utilised to estimate fault dimensions and slip values (D) based on the relationship between seismic moment (Mo), rigidity (μ), and fault area (A), given by $Mo = \mu \cdot A \cdot D$. The fault parameters, fault dimensions, slip values, and friction coefficients for each fault segment are listed in Table 1. The ΔCFS distribution pattern triggered by the three fault segments was computed, as depicted in Figure 6, showing a direct proportionality between the positive ΔCFS pattern and the areas of high density as derived from gravity analysis.

5. Gravity anomaly analysis

5.1. Bouguer gravity anomalies

The observed Bouguer anomalies (Figure 7a) reflect subsurface density changes, including the crust-upper mantle discontinuity. The map shows different wavelengths due to different subsurface densities, with a general increase from −70 mGal to 40 mGal towards the west. Notably, the overall upward trend towards the west aligns with the crustal configuration of a passive margin, as evidenced by the gradual

Table 1. The fault parameters that identified three fault segments used in calculating the coulomb stress change.

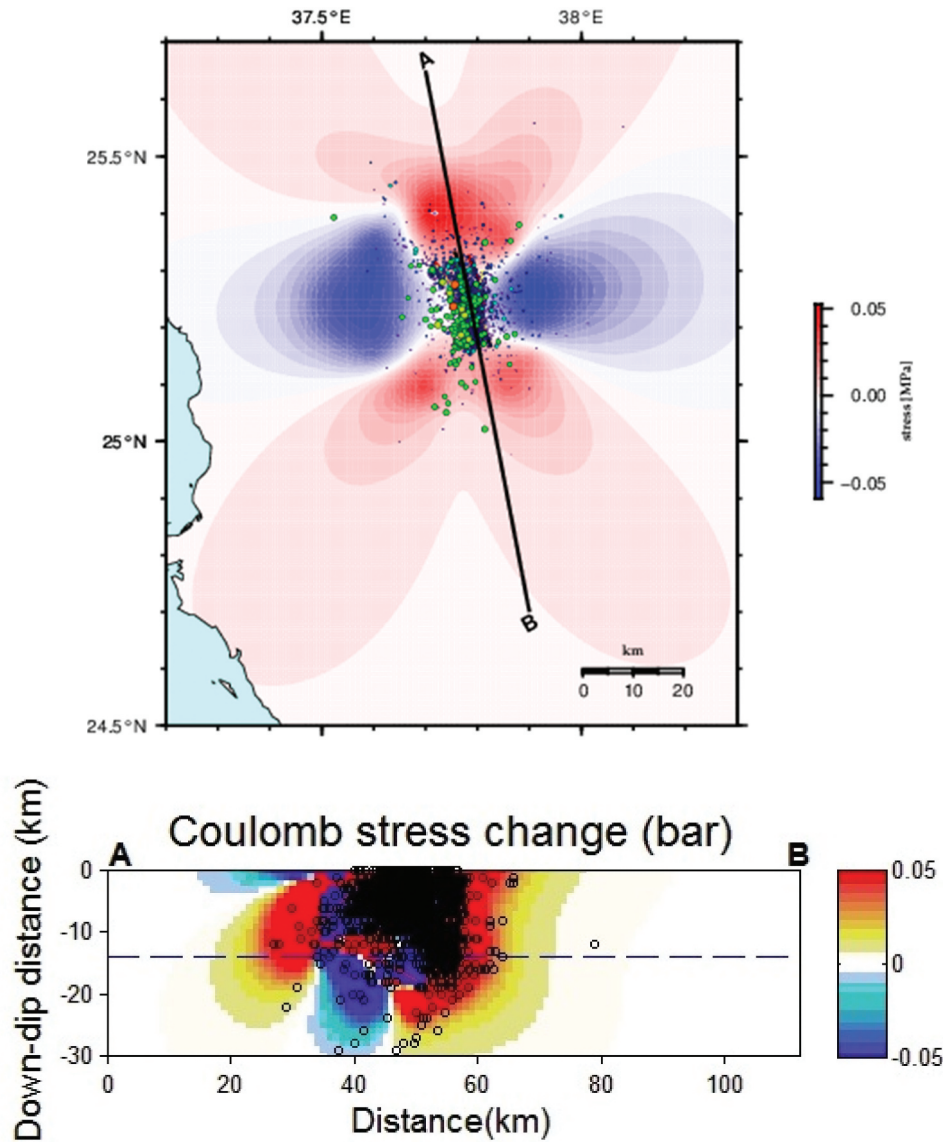| Fault zone	Fault area [m²]	Length [km]	Width [km]	ΣM_o [Nm]	M_w	$\Delta\sigma$ (MPa)	Strike [°]	Dip [°]	Rake [°]	Focal depth [km]	Depth range
1	173	6	8	6.92E + 23	5.2	5.9	133.3	87.8	−165.2	12	10–18
2	628	12.5	8	1.72E + 24	5.5	0.3	157.4	68.2	−77.5	6	1–9
3	163	4	7	7.41E + 22	4.5	0.7	185.6	74.9	−83.3	14	10–18

Figure 6. Coulomb failure stress calculated for three fault segments using the fault parameters listed in table 1. Higher positive values of coulomb failure stress change indicate the expected location of seismicity. The epicentres (coloured circles) and hypocentres (open circles) are projected on the map and cross-section plot.

thinning of the crust towards the Red Sea. The crustal thinning is described by many authors (Abdelfattah et al., 2021; Al-Damegh et al., 2005; Hansen et al., 2007). To effectively examine the effect of crustal heterogeneities, we derived a regional anomaly representing the effect of crust/mantle discontinuity. Since the crust/mantle discontinuity is profound, about 30 km deep (Hansen et al., 2007), it would be expressed by a smooth surface that could be obtained using the polynomial method. We computed various polynomial surfaces from the observed Bouguer values. Using the method proposed by Gabtni and Jallouli (2017), the optimal polynomial surface, considered regional and fitting the long wavelength, is a third-degree polynomial surface. This regional anomaly is then subtracted from the observed Bouguer anomalies to yield a residual (Figure 7b).

5.2. Residual anomaly analysis

Figure 7b shows the residual anomaly map obtained by subtracting the regional anomaly from the observed Bouguer anomaly. It represents the effect of different densities within the uppermost crust of the study area, the Cenozoic volcanic rock. The residual shows a repetitive prominent NE-SW anomaly. These anomalies have a width of about 30 km and an amplitude of 10 to 20 mGal. A critical inquiry arises regarding the origin of the noticeable NE-SW gravity anomalies, which are not parallel with the Red Sea rifting. Considering their wavelength, which is 30 km wide with an extent of 50 to 100 km, and considering the geological context of the study area, these anomalies reflect the Precambrian basement heterogeneities of the Arabian Shield. To clarify the cause of the gravity
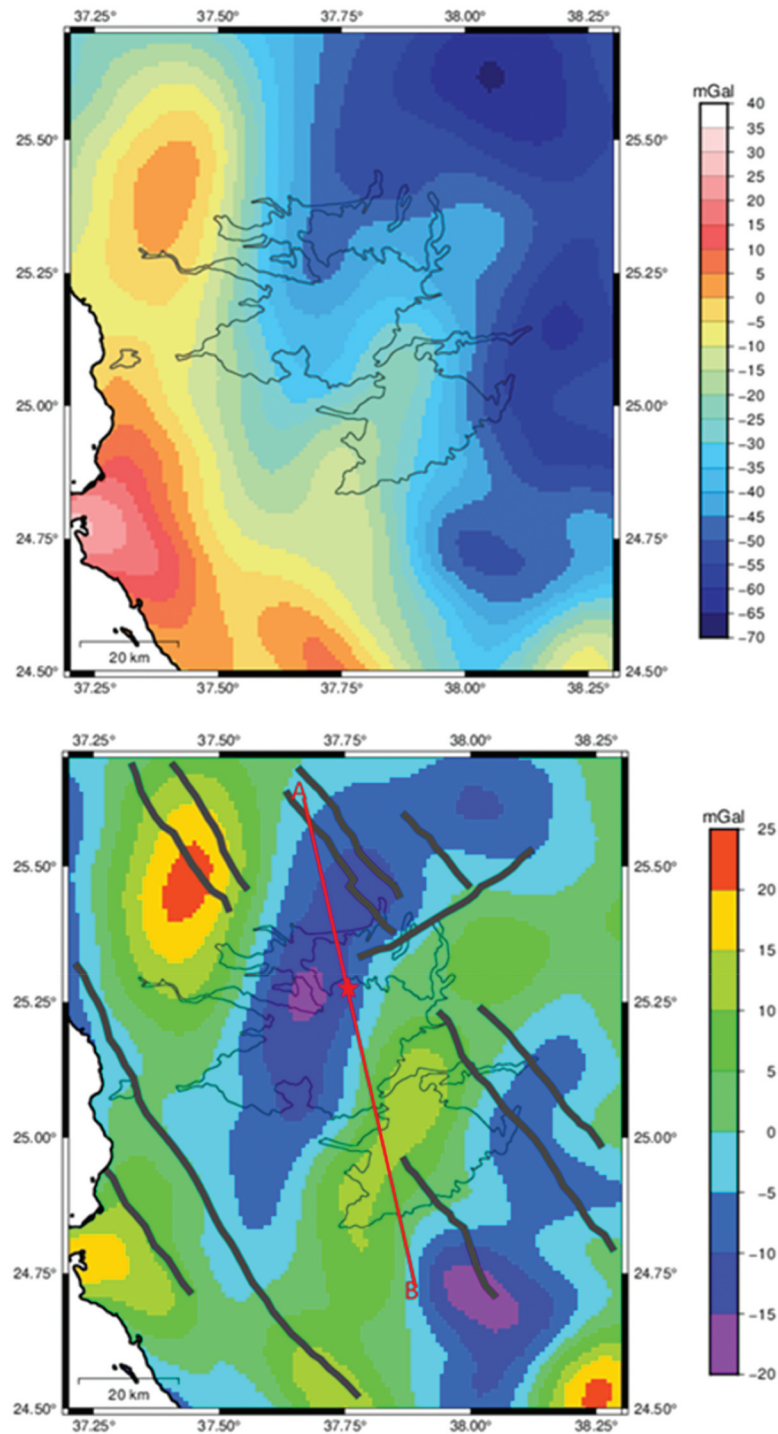
Figure 7. (top): bouguer anomaly map of HL area. Observed anomalies reflect all density contrasts in the subsurface. (bottom): residual anomaly map obtained after extraction of a regional. Values are in mGal. Red line indicates the location of the modeled profile (fig 8), red star represents the epicentre of the earthquake's 2009 main shock, thick grey lines represents dykes derived from the magnetic anomalies (Abdelfattah et al., 2020), thin grey line represents location of the harrat.

anomaly, we have marked the location of the NE-SW positive anomaly on the geological map (Figure 2). It is evident that the anomaly corresponds to the Proterozoic basement rocks represented by peridotite, serpentinite, diorite, and gabbro, all of which are high-density rocks underlying the Harrath. The presence of serpentine minerals refers to ultramafic rocks that could be associated to slices of oceanic crust or ophiolite complexes in Yanbu suture shown in Figure 1.

Hence, the identified NE-SW prominent gravity anomalies are associated with variations in physical properties, such as density, within the Precambrian basement.

5.3. Gravity modeling

The observed SW-NE residual anomalies associated with crustal heterogeneities are significant. Using edge detector filters based on gradients of potential

field anomalies, Abdelfattah et al. (2021) delineated SW-NE to SSW-NNE trends corresponding to boundaries of different basement blocks with different compositions and densities. To better image the subsurface, we applied a 2D modelling approach using inversion of the observed gravity anomalies. As the main objective of this study is to understand the generation mechanism of earthquakes, we selected a NW-SE profile crossing the seismogenic zone of HL for modelling (Figure 7). The 2D gravity model is constructed using the ZONDGM2D software (http://zond-geo.com/english/zond-software/gravity-magnetic-self-potential/zondgm2d/) (Figure 8). As gravity modelling is not unique, and we can propose different scenarios of density changes to explain the observed data, we need constraints from geologic observations or results from other geophysical data. The geologic map shows a Cenozoic basalt outcrop known by HL that flows over the Precambrian basement rocks, considering the most recent geologic feature in the study area. However, this feature is not expressed by a particular gravity anomaly. Even after removing the regional trend, the remaining residual do not fit the shape of the Cenozoic basalt outcrops, indicating that the surface basalt rocks are thin and do not exhibit a substantial density contrast with the underlying Precambrian basement rocks.

The gravity profile shows alternative negative and positive anomalies. The observed residual anomaly may be explained by heterogeneity within the basement, suggesting increasing density towards the southeast. However, based on S-wave tomography inversion (Koulakov et al., 2014; Lim et al., 2020; Tang et al., 2019), there is evidence of a low-velocity zone beneath HL under the observed positive gravity anomaly. Koulakov et al. (2014) constructed tomography

cross-sections that distinctly depict a low-velocity zone with a high Poisson ratio at a depth of more than 5 km. The S-wave velocity anomaly in this area reaches −120 m/s (Lim et al., 2020). This low-velocity zone corresponds to a low-density material. M. Mukhopadhyay et al. (2022) established the correlation between density (ρ) and the velocity Vs for the upper crust beneath the HL, indicating a linear regression:

$$\rho = 0.516 Vs + 1.204$$

Utilising this formula, a velocity anomaly of −120 m/s corresponds to a density variation of −0.06 g/cm³. So, using the S-wave tomography result as a constraint for gravity modelling, we have to consider the existence of a low-density zone at a depth of more than 5 km in the eastern zone, beneath the positive gravity anomaly, with a density contrast up to −0.06 g/cm³. Considering the reference density (2.67 g/cm3) used to calculate the Bouguer anomaly, the density range beneath HL would fall between 2.61 g/cm³ and 2.74 g/cm³. This range fits the density estimated by M. Mukhopadhyay et al. (2022) from receiver function analysis. The constructed model along the NW-SE profile illustrates crustal density changes beneath HL (Figure 8). The model crosses the active seismic zone (Figure 8). The negative anomaly observed on the NW side is attributed to relatively low-density basement rocks. In contrast, the positive anomalies observed on the SE side suggest the presence of high-density rocks. However, seismic tomography results (Koulakov et al., 2014) indicate a low-velocity zone beneath the observed positive gravity anomaly. Considering these constraints and the density contrast range inferred from the S-wave velocity anomaly, the positive anomaly is explained by a low-density material overlaid by
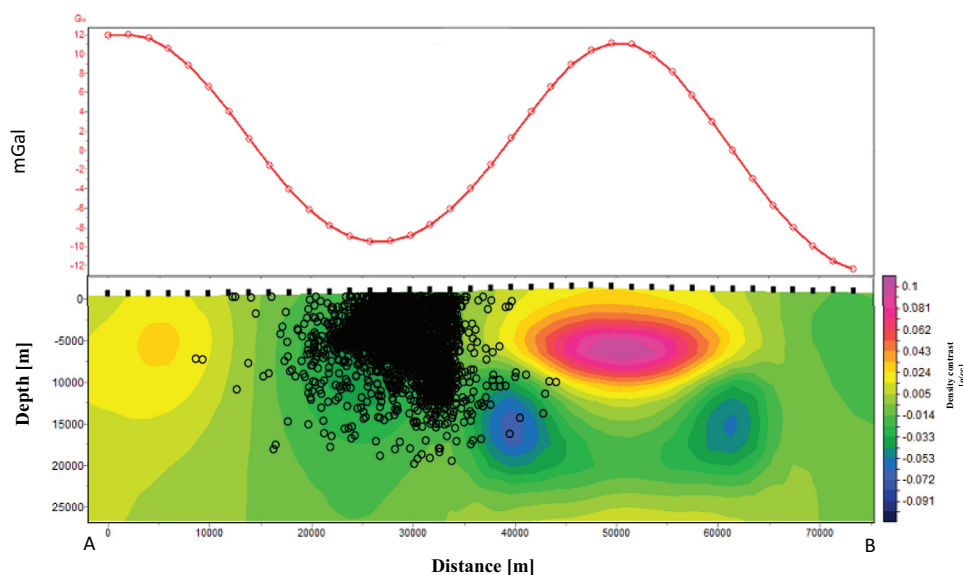

Figure 8. A 2D gravity model along an NW-SE profile. The model illustrates density changes in the subsurface that are related to the observed gravity anomaly. The black open circles indicate the spatial distribution of hypocentres along the cross-section.

dense rocks, with a density contrast of around 0.06 g/cm^3 (Figure 8). Considering the geological observations (Figure 2), these dense rocks correspond to Proterozoic ultramafic material represented by serpentinite, diorite and gabbro, underlying the Cenozoic Harrath rocks.

6. Results and discussions

Understanding these crustal heterogeneities is essential for comprehensively analysing earthquake processes in the Red Sea region, characterised by randomly distributed peculiar seismicities along onshores. The complex geological and tectonic features make an in-depth exploration of crustal heterogeneities crucial for unravelling the underlying factors influencing seismic activities and their distribution patterns in the region. Multi-step analysis has been performed to investigate depth-dependent distribution in density (as inferred from two-dimensional modelling of gravity and topography observations), earthquake source parameters (hypocentres, seismic moment, and stress drop), friction properties, and coulomb failure stress changes.

6.1. Hypocenter distributions

Figure 4 displays the spatial distribution of hypocentres in relation to magnitudes. The distribution of hypocentres implies that the unrest initially with larger-magnitude events began at deeper depths and subsequently progressed upward along the NS orientation, culminating in its peak with the most substantial event occurring at a shallower depth of 6 km, followed by subsequent smaller-magnitude events. This unrest is associated with the occurrences of surface fractures. As indicated by hypocentre distributions, the seismic activity appeared to occur within a low-density region bordered by a high-density zone (rigid patch). This rigid patch potentially serves as a solid asperity or barrier isolating the earthquake-prone zones, that may lead to future seismic events distributed along the NNE-SSW trend. Additionally, the manifestations of surface fractures associated with the unrest indicated that no features in the magma budget or hardness zones along the seismogenic zone prevent the flow of magma onto the Earth's surface, as suggested by earlier studies. The recent study by Huang et al. (2024) posits a strong relationship between magma activity and failure in the lower crust, implying that the triggering mechanisms for the observed earthquakes may be fundamentally linked to mantle upwelling.

The association of seismicity with zones characterised by low density can be attributed to various geological processes and tectonic settings. The presence of low-density materials in the Earth's crust can influence the behaviour of the crust and contribute to the occurrence of seismic events. Regions undergoing extensional tectonics that stretch and thin the Earth's crust are characterised by low-density rocks, such as those found in rift zones or areas of continental extension, which can experience faulting and seismicity (Buck, 1991). On the other hand, volcanic regions often contain low-density materials associated with magma chambers and volcanic rocks. The movement of magma and the associated tectonic processes can induce seismic events (Pollard & Segall, 1987). The respective dislocation zone is occupied in the Arabian Shield, where the geodynamic process is presumably believed to experience a coupling of tectonic and magmatic activities, potentially leading to seismic activity across various dislocation zones.

6.2. Seismic moments and stress-drops

Understanding the spatial distribution of seismic moments during earthquake unrest provides valuable insights into the dynamic processes preceding significant seismic events. Figure 5 illustrates the spatial distribution of HL's seismic moments released during the 2009 earthquake unrest. The figure reveals two distinct patches of high seismic moments. The first patch, associated with an event of Mw 5.0, occurred at a depth of 14 km 2 hours before the largest seismic event. The second patch corresponds to the most prominent event of Mw 5.4, shedding light on the complex dynamics leading to seismic activity in the region. Figure 5 reveals a spatial distribution of seismic moments aligned around the seismicity area.

Three distinct subzones were delineated based on the spatial distribution of hypocentres, the faulting styles derived from the focal mechanism solutions of Abdelfattah et al. (2021), and the triangle diagram obtained based on the method of Frohlich (2001). These subzones represent the preshock phase, comprised of 525 events occurring at depths between 10 and 20 km with magnitudes ranging from −0.4 to 5.2. The mainshock phase included 3,678 events at 2–10 km depths with local magnitudes ranging from −0.6 to 5.4. The aftershock phase represented 783 aftershocks distributed eastward and beneath the mainshock area at depths ranging from 10 to 20 km and local magnitudes between −0.7 and 4.0.

The stress drops associated with these phases are 5.9 MPa for the preshock phase, 0.3 MPa for the mainshock phase, and 0.7 MPa for the aftershock phase, implying that higher stress drops are associated with seismic events released during the initial phase compared to the other two phases within the seismogenic zone, emphasising that the foreshocks released the most of the stress around the fault zone and stopping by a dyke as suggested by Abdelfattah

et al. (2019). The representations of seismic moments and stress drops suggest that the rupture process initiated with larger event magnitudes at depths between 12 and 25 km. This release led to the redistribution of stress, concentrating around a localised aseismic deformation (asperity), which eventually discharged its strain with the occurrence of the largest event, a magnitude of 5.4, within the unrest, situated at a depth of 6 km. The calculations of stress drops presented in this study are in the range that was determined by previous studies. Abdelfattah et al. (2019) indicated that the foreshock stage was generally characterised by higher stress drops than the mainshock and aftershock phases, with stress drops ranging from about 0.6MPa and 22.3MPa. Furthermore, three southern Red Sea earthquakes exhibited stress drops ranging from 0.3 to 5.0 MPa (Kebede & Van Eck, 1990). The calculated stress drop of the 16 June 2020 ML 5.4 earthquake, northern Red Sea, was exhibited to vary from 0.02 to 13 MPa (Saadalla and Hamed). Finally, the stress drop of the preshock phase, which is relatively high, is consistent with the suggestion of Baer and Hamiel (2010), Pallister et al. (2010), and B. Mukhopadhyay et al. (2012), who attributed the swarm activity to dike intrusions. On the other hand, the stress drops of the mainshock phase are consistent with those related to ambient tectonics.

7. Friction coefficient

The friction coefficient μ' is a dimensionless parameter that characterises the resistance to sliding across fault planes. A friction coefficient ranging from 0.4 to 1.0 signifies diverse levels of frictional resistance along the faults. A coefficient below 0.4 generally indicates low resistance to sliding, suggesting smoother fault interfaces, reduced roughness, or the presence of lubricating substances. A low friction coefficient may be associated with cohesive soils or well-lubricated fault zones in geotechnical engineering. Friction coefficients within the 0.4 to 1.0 range indicate moderate to high resistance to sliding, encompassing the typical spectrum for many common materials, including construction materials, rocks, and soils. A greater value within this range indicates increased frictional resistance. The 0.4 to 1.0 range suggests variability in frictional conditions, where different materials within a system may exhibit distinct coefficients based on factors like surface roughness, moisture content, and environmental conditions. A friction coefficient of 1.0 signifies the maximum possible resistance to sliding along fault planes, indicating that the fault interface provides the highest achievable frictional resistance, which might occur when fault surfaces are rough, dry, and in direct contact.

7.1. Coulomb stress failure

The three fault segments used for Coulomb stress modelling were likely defined through the spatiotemporal distribution of Hypocenters, stress tensor inversion of focal mechanism solutions obtained by Abdelfattah et al. (2021), and the triangle diagram of focal mechanisms depicted in Figure 4b obtained based on the method of Frohlich (2001). These solutions provide insights into the orientations and magnitudes of principal stresses associated with earthquake events. Additionally, the orientation of the AB profile line relative to dyke intrusions and surface fractures, as defined by previous studies (Abdelfattah et al., 2021, 2022; Baer & Hamiel, 2010; Pallister et al., 2010;), that is consistent with the distribution of epicentres on the map in Figure 4. The strike of the AB profile, as depicted in Figure 4, was likely established by aligning the profile line with prominent geological features or structural trends in the study area.

Interpreting the Coulomb stress map involves identifying and evaluating the sites where the potential future seismic rupture can occur. Specifically, the analysis scrutinises areas with increased Coulomb stress, acting as indicators of highlight seismic risk where future seismic events may occur, providing valuable insights for earthquake hazard assessment and mitigation efforts.

Previous studies conducted on the epicentral area, utilising satellite interferometry, revealed a connection with dyke injection parallel to the margin of the Red Sea (Baer & Hamiel, 2010; Pallister et al., 2010). The epicentres were oriented along the NNW trend. Hypocenters were categorised into three fault segments based on hypocentral distributions and focal mechanism solutions derived by Abdelfattah et al. (2021): preshock segment, mainshock segment, and aftershock segment located in the southward, shallower events northward, and eastward of the mainshock and preshock phases. The distribution of hypocentres, along with surface deformations, lends support to the dyke intrusion model beneath the epicentral area.

The Coulomb stress changes resulting from the three fault segments during the unrest of the 2009 hL earthquakes exhibit distributions as depicted in Figure 6. These changes include Coulomb stress increases induced by the unrest at the fault tips parallel to the Red Sea. Positive lobes of Coulomb failure stress indicate regions where stress accumulation raises the likelihood of future earthquake occurrence. When Coulomb failure stress surpasses a critical threshold, it can trigger fault slip and generate earthquakes. Positive lobes represent areas where stress conditions favour faulting due to tectonic loading or stress transfer from previous seismic events. Understanding the spatial distribution of positive stress lobes is crucial for

seismic hazard assessment and earthquake forecasting. By identifying zones of heightened stress accumulation, we can identify locations at higher risk of seismic activity. This result can provide valuable guidance for emergency preparedness initiatives, land use planning, and infrastructure resilience strategies to reduce future earthquake impacts.

The Coulomb failure stress change exhibits two distinct areas of positive stress, known as stress lobes, which have the potential to induce future seismic activity. One stress lobe follows a north-northwest (NNW) trend, while the other follows a northeast (NE) trend. Artemieva et al. (2022) provided a tectonic model indicating that the Red Sea axial rift can be expanded further into the Arabian Shield due to an offset migration related to the relative tectonic movement between the Arabian and African plates. This model identifies the NNW trend as a fault accumulating stress, suggesting that future earthquakes may occur along this fault. Therefore, NNW-oriented faults undergo substantial stress build-up and have the potential to rupture, leading to seismic occurrences in the study area. Positive Coulomb failure stress change corresponds to positive gravity anomalies, indicating an expected location for forthcoming seismic activity in the region. Abdelfattah et al. (2020, 2021; 2022) suggested that stress accumulates and transfers through transverse faults corresponding to the NE fault trends, activating the NNW fault trend inside the Arabian Shield. This NNW fault trend parallels the Red Sea axial rift within the Arabian Shield.

The positive stress lobes identified in the stress map (Figure 6) indicate regions where stress is accumulating, suggesting a higher potential for seismic activity. These lobes are spatially distributed along two directions: the NNW-SSE direction and the NNE-SSW direction, respectively, suggesting the potential occurrence of future earthquakes. However, the absence of earthquakes implies that the accumulated stress has not yet reached the necessary threshold to initiate rupture on the existing fault. It is possible that existing barriers or asperities in the region are inhibiting the release of stress, thereby preventing earthquakes from occurring. This interplay between stress accumulation and the mechanical properties of the fault system underscores the complexity of seismic behaviour in the area. Understanding these dynamics is crucial for improving models of anticipating future activity.

7.2. Gravity analyses

Gravity anomalies indicate density heterogeneities within the crust of the HL seismogenic zone and its surrounding vicinity. By examining the spatial arrangement and intensity of these anomalies, we can identify geological boundaries, decipher structural patterns, and deduce the volcanic evolution of the area.

Furthermore, combining gravity data with other geophysical methods like magnetic, seismic and ground-penetrating radar offers a holistic understanding of the subsurface structure. Understanding gravity anomalies necessitates meticulous examination and correlation with additional geological information. Positive anomalies often signal the existence of denser materials. Indeed, the observed SW-NE positive gravity anomaly in the study area is linked to peridotite, serpentinite and gabbro rocks that constitute a portion of the Precambrian basement with high density. The high-density mass patch indicates localised stress concentration areas that may break. Conversely, decreased anomalies may point to less dense rocks, indicating regions of dense fractures where earthquakes were potentially triggered. The study area is covered by magnetic data analysed in previous studies (Abdelfattah et al., 2021; Rashed et al., 2020; Zahran et al., 2017). The magnetic maps show different NW-SE trends that correspond to recent geological features represented by NW-SE faults and dykes associated to the Red Sea rift. These recent detailed features evidenced by magnetic maps are not shown in gravity maps derived from World Gravity models.

This study emphasises the importance of understanding crustal heterogeneities and stress accumulation mechanisms for forecasting and preparing for future seismic events within seismogenic zones. The crustal heterogeneities within the HL significantly contribute to the complexity and roughness of the geological setting where seismic events occur. The geologic and gravity maps show clearly the high degree of heterogeneity and variation of crustal composition of the Precambrian basement where we may find even ultramafic rocks in some localities that refer to the presence of slices of oceanic crust or ophiolite complexes, expressed in the study area by SW-NE positive gravity anomaly. Such dense and rigid rocks can manifest as barriers and asperities, which play pivotal roles in the accumulation of stress and the subsequent behaviour of faults. As articulated by Aki (1984), barriers are geological features that inhibit fault movement due to higher frictional strength or density, while asperities are specific points along a fault where stress accumulates prior to a rupture. In the context of the HL region, the presence of these structures can be interpreted through the analysis of high-density anomalies associated with magmatic bodies. These high-density regions may serve as solid patches that isolate earthquake-prone zones, potentially leading to a concentration of future seismic events. Hypocenter distributions within the HL region indicate that seismic activity tends to occur within lower-density regions bordered by high-density zones along an NNE-SSE trend. This configuration suggests that the rigid patches surrounding these low-density areas could function as asperities or barriers, effectively

isolating and containing stress accumulation within the earthquake-prone zones. Additionally, the observed seismicity aligns with a distinct NNE-SSW trend, indicating a preferred orientation for faulting mechanisms influenced by regional tectonic stresses. The analysis of Coulomb failure stress changes reveals the presence of four lobes of positive failure stress, pinpointing areas where stress accumulation is likely to influence future seismic activity. These lobes signify potential zones of rupture, highlighting the relationship between stress distribution and the likelihood of future earthquakes. Furthermore, the identified crustal heterogeneities, characterised by the juxtaposition of high-density regions related to positive gravity anomalies, adjacent to previously ruptured fault zones, accentuate the interplay between tectonic dynamics and seismic hazards, suggesting areas that are more susceptible to future earthquakes. Integrating insights regarding crustal heterogeneities in the HL region provides a clearer understanding of the mechanisms that govern local seismicity. The interplay of barriers and asperities, coupled with the analysis of stress changes and density variations, underscores the susceptibility of certain areas to future seismic events.

This study emphasises the importance of understanding crustal heterogeneities and stress accumulation mechanisms for forecasting and preparing for future seismic events within seismogenic zones. Integrating gravity anomalies, earthquake characteristics, and Coulomb stress transfer has elucidated critical relationships between the observed seismic activity and the underlying geological features. Notably, the characterisation of the NNW-aligned faults, including the HL fault segments, has revealed significant positive Coulomb stress patterns that correlate with the HL seismic activity. Furthermore, the identified crustal heterogeneities, characterised by high-density regions adjacent to the ruptured fault zones, reinforce the connection between tectonic dynamics and seismic hazards, indicating areas that are more susceptible to future earthquakes are likely to occur. These findings emphasise the importance of these fault segments as key contributors to the potential seismic hazard in the region and highlight the need for ongoing monitoring of these critical geological structures.

8. Conclusions

This study examined two primary factors influencing the dynamic rupture of potential future earthquakes: crustal heterogeneities and coseismic Coulomb failure stress in the epicentral area of HL following the release of the 2009 earthquake unrest. To achieve this study, we integrated gravity analysis, hypocentre spatial distribution, seismic moments, stress drops, frictional properties, and Coulomb stress transfer to reveal

significant crustal heterogeneities and ongoing stress concentrations.

The spatial distribution of hypocentres and associated surface fractures indicated no noticeable features in the magma budget or hardness zones within the seismogenic zone that could impede magma flow to the surface. Coulomb failure stress analysis demonstrated positive lobes distributed along the northnorthwest (NNW) fault trend, which parallels the axial rift of the Red Sea. The relationship between spatial heterogeneities in density materials and the positive stress concentrations derived from Coulomb failure stress analysis indicates their potential impact on the rupture dynamics of future earthquakes in HL. Gravity analysis revealed spatial heterogeneities ranging from low- to high-density materials within the seismogenic zone. Notably, the spatial correlation between hypocentres and low-density areas highlights the influence of subsurface density on seismic activity, contributing to a better understanding of regional seismic patterns and implications for earthquake hazard assessments in similar geological environments.

Based on the current analyses, we propose a rupture process scenario for the 2009 earthquake unrest, initiated with stress accumulation at depths between 12 and 25 kilometres. This accumulation leads to stress redistribution, culminating in the release of the most significant event, a magnitude 5.4 earthquake, occurring at a depth of 6 kilometres within the zone of unrest. By leveraging insights from identified crustal heterogeneities as informed by gravity analyses and the pattern of lobes of Coulomb failure stress, our findings suggest a scenario indicating the likelihood of future earthquake occurrences in regions where stress accumulation increases in conjunction with positive lobes of Coulomb failure stress and high-density areas characterised by positive gravity anomalies.

This study emphasises the importance of understanding crustal heterogeneities and stress accumulation mechanisms for forecasting and preparing for future seismic events within seismogenic zones. The crustal heterogeneities within the HL significantly contribute to the complexity and roughness of the geological setting where seismic events occur. These variations in crustal composition and structure can largely be attributed to the intrusion of magmatic activity into the upper layers of the Earth's crust. Such intrusions can manifest as barriers and asperities, which play pivotal roles in the accumulation of stress and the subsequent behaviour of faults. As articulated by Aki (1984), barriers are geological features that inhibit fault movement due to higher frictional strength or density, while asperities are specific points along a fault where stress accumulates prior to a rupture. In the context of the HL region, the presence of these structures can be interpreted through the analysis of high-density anomalies associated

with intrusive magmatic bodies. These high-density regions may serve as solid patches that isolate earthquake-prone zones, potentially leading to a concentration of future seismic events. The significance of these geological structures, including asperities and barriers, is closely related to volcanic structures and local seismicity, as suggested in studies of the area (Abdelfattah et al., 2017). Seismic hypocentre distributions within the HL region indicate that seismic activity tends to occur within lower-density regions bordered by high-density zones along an NNE-SSE trend. This configuration suggests that the rigid patches surrounding these low-density areas could function as asperities or barriers, effectively isolating and containing stress accumulation within the earthquake-prone zones. Additionally, the observed seismicity aligns with a distinct NNE-SSW trend, indicating a preferred orientation for faulting mechanisms influenced by regional tectonic stresses. The analysis of Coulomb failure stress changes reveals the presence of four lobes of positive failure stress, pinpointing areas where stress accumulation is likely to influence future seismic activity. These lobes signify potential zones of rupture, highlighting the relationship between stress distribution and the likelihood of future earthquakes. Furthermore, the identified crustal heterogeneities, characterised by the juxtaposition of high-density regions related to positive gravity anomalies, adjacent to previously ruptured fault zones, accentuate the interplay between tectonic dynamics and seismic hazards, suggesting areas that are more susceptible to future earthquakes. Integrating insights regarding crustal heterogeneities in the HL region provides a clearer understanding of the mechanisms that govern local seismicity. The interplay of barriers and asperities, coupled with the analysis of stress changes and density variations, underscores the susceptibility of certain areas to future seismic events. This knowledge is crucial for enhancing predictive models of seismic hazards in the HL, ultimately contributing to improved monitoring and risk mitigation strategies.

Acknowledgments

Disclosure statement

No potential conflict of interest was reported by the author(s).

Funding

ORCID

Ali Abdelfattah 🔟 http://orcid.org/0000-0001-7732-6998

References

Abdelfattah, A. K., Abdelrahman, K., Qaysi, S., Fnais, M., & Al-Amri, A. (2022). Earthquake recurrence characteristics for potential seismic zones in the southern Red Sea region and their hazard implications on Jizan city. *Journal of King Saud University-Science*, *34*(3), 101880. https://doi.org/10.1016/j.jksus.2022.101880

Abdel-Fattah, A. K., Al-Amri, A. M., Fnais, M. S., & Abdelrahman, K. (2014). Estimation of source parameters and attenuation using digital waveforms of Al-ays 2009 earthquake, Saudi Arabia. *Arabian Journal of Geosciences*, *7*(8), 3325–3337. https://doi.org/10.1007/s12517-013-1021-3

Abdelfattah, A. K., de Lorenzo, S., Almadani, S., Fnais, M., Alfaifi, H., & Al-Arifi, N. (2019). Another look at the 2009 seismic activity, Harrat Lunayyir, Saudi Arabia. *Journal of Seismology*, *23*(4), 801–818. https://doi.org/10.1007/s10950-019-09835-0

Abdelfattah, A. K., Jallouli, C., Fnais, M., Qaysi, S., Alzahrani, H., & Mogren, S. (2021). The key role of conjugate fault system in importing earthquakes into the eastern flank of the Red Sea. *Earth Planets & Space*, *73*(1), 1–19. https://doi.org/10.1186/s40623-021-01513-1

Abdelfattah, A. K., Jallouli, C., Qaysi, S., & Al-Qadasi, B. (2020). Crustal stress in the Northern Red Sea Region as inferred from seismic b-values, seismic moment release, focal mechanisms, gravity, magnetic, and heat flow data. *Surveys in Geophysics*, *41*(5), 963–986. https://doi.org/10.1007/s10712-020-09602-8

Abdelfattah, A. K., Mogren, S., & Mukhopadhyay, M. (2017). Mapping b-value for 2009 harrat lunayyir earthquake swarm, western Saudi Arabia and coulomb stress for its mainshock. *Journal of Volcanology and Geothermal Research*, *330*, 14–23. https://doi.org/10.1016/j.jvolgeores.2016.12.001

Aki, K. (1984). Asperities, barriers, characteristic earthquakes and strong motion prediction. *Journal of Geophysical Research Solid Earth*, *89*(B7), 5867–5872. https://doi.org/10.1029/JB089iB07p05867

Aki, K., & Richards, P. (1980). *Quantitative seismology: Theory and methods* (p. 557). Freeman Co., San Francisco.

Al-Damegh, K., Sandvol, E., & Barazangi, M. (2005). Crustal structure of the Arabian plate: New constraints from the analysis of teleseismic receiver functions. *Earth and Planetary Science Letters*, *231*(3–4), 177–196. https://doi.org/10.1016/j.epsl.2004.12.020

Alkan, H., Öztürk, S., & Akkaya, İ. (2023). Seismic Hazard implications in and around the Yedisu seismic gap (eastern türkiye) based on coulomb stress changes, b-values, and S-wave velocity. *Pure & Applied Geophysics*, *180*(9), 3227–3248. https://doi.org/10.1007/s00024-023-03342-7

Al-Zahrani, H. A., Fnais, M. S., Al-Amri, A. M., & Abdel-Rahman, K. (2012). Tectonic framework of Lunayyir area, northwest Saudi Arabia through aftershock sequence analysis of

19 May 2009 earthquake and aeromagnetic data. *International Journal of Physical Sciences*, 7(44), 5821–5833.

Aoyama, H., Ide, S., & Shibazaki, B. (2000). Coulomb stress triggering of the 1997 Kagoshima earthquakes by the 1996 earthquake at hyuga-nada. *Geophysical Research Letter*, 27(10), 1475–1478.

Artemieva, I. M., Yang, H., & Thybo, H. (2022). Incipient ocean spreading beneath the Arabian shield. *Earth-Science Reviews*, 226 (2022) 103955. https://doi.org/10.1016/j.earscirev.2022.103955

Baer, G., & Hamiel, Y. (2010). Form and growth of an embryonic continental rift: InSAR observations and modeling of the 2009 western Arabia rifting episode. *Geophysical Journal International*, 182, 155–167. https://doi.org/10.1111/j.1365-246X.2010.04627.x

Bhattacharya, P. M., & Kayal, J. R. (2003). Mapping the b-value and its correlation with the fractal dimension in the northeast region of India. *Geological Society of India* 62(6), 680–695.

Bonvalot, S., Balmino, G., Briais, A., Kuhn, M., Peyrefitte, A., Vales, N., Biancale, R., Gabalda, G., & Reinquin, F. (2012). World Gravity Map: A set of global complete spherical bouguer and isostatic anomaly maps and grids. EGU general assembly conference abstracts. Vienna.

Buck, W. R. (1991). Modes of continental lithospheric extension. *Journal of Geophysical Research Solid Earth*, 96 (B7), 20161–20178. https://doi.org/10.1029/91JB01485

Chen, X., Shearer, P. M., & Abercrombie, R. E. (2012). Spatial migration of earthquakes within seismic clusters in Southern California: Evidence for fluid diffusion. *Journal of Geophysical Research Solid Earth*, 117(B4). https://doi.org/10.1029/2011JB008973

Fnais, M. S., Abdelrahman, K., & Al-Amri, A. M. (2010). Microtremor measurements in Yanbu city of Western Saudi Arabia: A tool for seismic microzonation. *Journal of King Saud University-Science*, 22(2), 97–110. https://doi.org/10.1016/j.jksus.2010.02.006

Frohlich, C. (2001). Display and quantitative assessment of distributions of earthquake focal mechanisms. *Geophysical Journal International*, 144(2), 300–308.

Gabtni, H., & Jallouli, C. (2017). Regional-residual separation of potential field: An example from Tunisia. *Journal of Applied Geophysics*, 137, 8–24. https://doi.org/10.1016/j.jappgeo.2016.12.011

Hanks, T. C., & Kanamori, H. (1979). A moment magnitude scale. *Journal of Geophysical Research Solid Earth*, 84(B5), 2348–2350. https://doi.org/10.1029/JB084iB05p02348

Hansen, S. E., DeShon, H. R., Moore-Driskell, M. M., & Al-Amri, A. M. (2013). Investigating the P wave velocity structure beneath Harrat Lunayyir, northwestern Saudi Arabia, using double-difference tomography and earthquakes from the 2009 seismic swarm. *Journal of Geophysical Research Solid Earth*, 118(9), 4814–4826. https://doi.org/10.1002/jgrb.50286

Hansen, S. E., Rodgers, A. J., Schwartz, S. Y., & Al-Amri, A. M. (2007). Imaging ruptured lithosphere beneath the Red Sea and Arabian Peninsula. *Earth and Planetary Science Letters*, 259(3–4), 256–265. https://doi.org/10.1016/j.epsl.2007.04.035

Harris, R. A. (1998). Introduction to coulomb stress triggering. *Journal of Geophysical Research Solid Earth*, 103(B11), 24447–24461.

Huang, K., Wei, G., Chen, K., Zhang, N., Li, M., & Dal Zilio, L. (2024). The 2023 mw 6.8 Morocco earthquake: A lower crust event triggered by mantle upwelling? *Geophysical Research Letter*, 51(12), e2024GL109052. https://doi.org/10.1029/2024GL109052

Johnson, P. R. (1998). Tectonic map of Saudi Arabia and adjacents areas (scale: 1: 4, 000, 000). *Saudi Arabian Deputy Ministry for Mineral Resources Open-File Report*, USGS-OF-97–3.

Johnson, P. R. (2006). *Explanatory notes to the map of Proterozoic geology of western Saudi Arabia. Saudi geological survey. Technical Report SGS-TR-2006-4*, 62 p. 22 fi gs. 2 plates.

Kebede, F., & Van Eck, T. (1990). Spectral source parameters for three earthquakes in the southern Red Sea - Paramètres de source de trois séismes dans la partie sud de la mer Rouge obtenus par analyse spectrale. *Physics of the Earth and Planetary Interiors*, 59(4), 288–293. https://doi.org/10.1016/0031-9201(90)90235-P

Khan, P. K., & Chakraborty, P. P. (2007). The seismic b-value and its correlation with bouguer gravity anomaly over the Shillong Plateau area: Tectonic implications. *Journal of Asian Earth Sciences*, 29(1), 136–147. https://doi.org/10.1016/j.jseaes.2006.02.007

King, G. C., Stein, R. S., & Lin, J. (1994). Static stress changes and the triggering of earthquakes. *Bulletin of the Seismological Society of America*, 84(3), 935–953.

Koulakov, I., El Khrepy, S., Al-Arifi, N., Sychev, I., & Kuznetsov, P. (2014). Evidence of magma activation beneath the harrat lunayyir basaltic field (Saudi Arabia) from attenuation tomography. *Advances in Fission-Track Geochronology*, 5(2), 873–882. https://doi.org/10.5194/se-5-873-2014

Koulakov, I., Kukarina, E., Fathi, I. H., El Khrepy, S., & Al-Arifi, N. (2015). Anisotropic tomography of Hokkaido reveals delamination-induced flow above a subducting slab. *Journal of Geophysical Research Solid Earth*, 120(5), 3219–3239. https://doi.org/10.1002/2014JB011823

Lim, J. A., Chang, S. J., Mai, P. M., & Zahran, H. (2020). Asthenospheric flow of plume material beneath Arabia inferred from S wave traveltime tomography. *Journal of Geophysical Research Solid Earth*, 125(8), e2020JB019668. https://doi.org/10.1029/2020JB019668

Madariaga, R., & Ruiz, S. (2016). Earthquake dynamics on circular faults: A review 1970–2015. *Journal of Seismology*, 20(4), 1235–1252. https://doi.org/10.1007/s10950-016-9590-8

Mereu, R. F. (2020). A study of the relations between ML, me, mw, apparent stress, and fault aspect ratio. *Physics of the Earth and Planetary Interiors*, 298, 106278. https://doi.org/10.1016/j.pepi.2019.106278

Mukhopadhyay, B., Mogren, S., Mukhopadhyay, M., & Dasgupta, S. (2012). Incipient status of dyke intrusion in top crust – evidences from the Al-ays 2009 earthquake swarm, Harrat Lunayyir, SW Saudi Arabia. *Geomatics, Natural Hazards and Risk*, 4(1), 1–19. https://doi.org/10.1080/19475705.2012.663794

Mukhopadhyay, M., Mukhopadhyay, B., Mogren, S., Nandi, B. K., & Ibrahim, E. (2022). Regional significance of crustal and sub-crustal rheological heterogeneities beneath the harrat lunayyir and their continuity into the neighboring harrats, Western Saudi Arabia – perspectives of the afar plume activity. *Journal of African Earth Sciences*, 186, 104432. https://doi.org/10.1016/j.jafrearsci.2021.104432

Okada, Y. (1992). Internal deformation due to shear and tensile faults in a half-space. *Bulletin of the Seismological Society of America*, 82(2), 1018–1040.

Pallister, J. S., McCausland, W. A., Jónsson, S., Lu, Z., Zahran, H. M., Hadidy, S. E., Aburukbah, A., Stewart, I. C. F., Lundgren, P. R., White, R. A., & Moufti, M. R. H. (2010). Broad accumulation of rift-related extension recorded by dyke intrusion in Saudi Arabia.

Nature Geosciences, 3(10), 705–712. https://doi.org/10.1038/NGEO966

Pollard, D. D., & Segall, P. (1987). Theoretical displacements and stresses near fractures in rock: With applications to faults, joints, veins, dikes, and solution surfaces. *Fracture Mechanics of Rock*, 277(349), 277–349.

Rashed, M., Zahran, H., Atef, A., Harbi, H., Al-Dhahry, M., & Al-Hady, S. (2020). A new perspective of the 2009 Al-ays earthquake episode at western Arabia. *Journal of Asian Earth Science*, 188, 104101. https://doi.org/10.1016/j.jseaes.2019.104101

Roland, E., & McGuire, J. J. (2009). Earthquake swarms on transform faults. *Geophysical Journal International*, 178(3), 1677–1690. https://doi.org/10.1111/j.1365-246X.2009.04214.x

Saibi, H., Mogren, S., Mukhopadhyay, M., & Ibrahim, E. (2019). Subsurface imaging of the harrat lunayyir 2007–2009 earthquake swarm zone, western Saudi Arabia, using potential field methods. *Journal of Asian Earth Sciences*, 169, 79–92. https://doi.org/10.1016/j.jseaes.2018.07.024

Schoenball, M., & Gröner, E. (2016). The role of barrier zones in the seismicity of regions with complex tectonics. *Geosphere*, 12(5), 1578–1589.

Stein, R. S., Barka, A. A., & Dieterich, J. H. (1997). Progressive failure on the North Anatolian fault since 1939 by earthquake stress triggering. *Geophysical Journal International*, 128(3), 594–604. https://doi.org/10.1111/j.1365-246X.1997.tb05321.x

Stein, R. S., King, G. C., & Lin, J. (1992). Change in failure stress on the southern San Andreas fault system caused by the 1992 magnitude= 7.4 landers earthquake. *Science*, 258 (5086), 1328–1332. https://doi.org/10.1126/science.258.5086.1328

Stern, R. J., & Johnson, P. R. (2019). Constraining the opening of the red sea: Evidence from the Neoproterozoic margins and Cenozoic magmatism for a volcanic rifted margin. *Geological Setting, Palaeoenvironment and Archaeology of the Red Sea*, 53–79. https://doi.org/10.1007/978-3-319-99408-6_4 .

Sychev, D. A., Otdelenov, V. A., Krasnova, N. M., & Ilyina, E. S. (2016). Polypragmasy: A clinical pharmacologist's view. *Terapevticheskii arkhiv*, 88(12), 94–102. https://doi.org/10.17116/terarkh2016881294-102

Tang, T., Shindell, D., Faluvegi, G., Myhre, G., Olivié, D., & Voulgarakis, A., Kasoar, M., Andrews, T., Boucher, O., Forster, P. M., Hodnebrog, Ø., Iversen, T., Kirkevåg, A., Lamarque, J.-F., Richardson, T., Samset, B. H., Stjern, C. W., Takemura, T.Smith, C. (2019). Comparison of effective radiative forcing calculations using multiple methods, drivers, and models. *Journal of Geophysical Research Atmospheres*, 124(8), 4382–4394. https://doi.org/10.1029/2018JD030188

Toda, S., & Enescu, B. (2011). Rate/State coulomb stress transfer model for the CSEP Japan seismicity forecast. *Earth Planets & Space*, 63(3), 171–185. https://doi.org/10.5047/eps.2011.01.004

Toda, S., & Stein, R. S. (2015). 2014 M w 6.0 South Napa earthquake triggered exotic seismic clusters near several Major faults. *Seismological Research Letters*, 86(6), 1593–1602. https://doi.org/10.1785/0220150102

Toda, S., Stein, R. S., Sevilgen, V., & Lin, J. (2011). Coulomb 3.3 graphic-rich deformation and stress-change software for earthquake, tectonic, and volcano research and teaching-user guide. *US Geological Survey Open-File Report*, 1060, (2011), 63.

Vavryčuk, V. (2014). Iterative joint inversion for stress and fault orientations from focal mechanisms. *Geophysical Journal International*, 199(1), 69–77. https://doi.org/10.1093/gji/ggu224

Zahran, H. M., El-Hady, S. M., & Abuelnaga, H. S. (2017). Aeromagnetic data over Harrat Lunayir and surrounding areas, western Saudi Arabia. *Arabian Journal of Geosciences*, 10(3), 1–15. https://doi.org/10.1007/s12517-017-2849-8

Zaidi, F. K., & Mukhopadhyay, M. (2015). Morphometric analysis of the scoria cones and drainage pattern for the quaternary and older volcanic fields in parts of the large igneous province (LIP), Saudi Arabia. *Journal of African Earth Sciences*, 110, 1–13. https://doi.org/10.1016/j.jafrearsci.2015.06.010

Zobin, V. M., Al-Amri, A. M., & Fnais, M. (2013). Seismicity associated with active, new-born, and re-awakening basaltic volcanoes: Case review and the possible scenarios for the Harraat volcanic provinces, Saudi Arabia. *Arabian Journal of Geosciences*, 6(2), 529–541. https://doi.org/10.1007/s12517-011-0379-3